Journal of Research in Ecology

An International Scientific Research Journal

Original research

Numerical simulation of effect of inflow Froude number on flow separation zone in junctions

Authors:
Farhad Majidian and Maaroof Siosemarde

Institution:
Department of Civil Engineering, Mahabad Branch, Islamic Azad University, Mahabad, Iran.

Corresponding author:
Maaroof Siosemarde

Email Id:
maroof-33m@yahoo.com

Web Address:
http://ecologyresearch.info/documents/EC00271.pdf

ABSTRACT:

Junctions are generally used in water distribution networks, irrigation channels, sewage networks, water/wastewater treatment facilities, input to power generation facilities, and etc. In this study, the flow numerical simulation has been performed in a 90^0 junction using RSM turbulence model. Water surface and flow velocity profiles at different sections of the main and lateral channels were compared with the experimental results and a good agreement has been found between them. Then, considering the good results obtained from previous sections, Froude number effect of the main and lateral channels entrance on flow separation zone was studied. The results showed that for a ratio of constant discharge, with approaching to channel bed, length of circulation zone is also decreased. Moreover, stream tube dimensionless width in water surface and bed were increased and decreased, respectively.

Keywords:

T-Junction, Flow Pattern, Inflow Froude number, Separation Zone, RSM turbulence model

Article Citation:
Farhad Majidian and Maaroof Siosemarde
Numerical simulation of effect of inflow Froude number on flow separation zone in junctions
Journal of Research in Ecology (2017) 5(1): 454 –463

Dates:
Received: 20 Jan 2017 **Accepted:** 21 Jan 2017 **Published:** 25 Feb 2017

Journal of Research in Ecology

INTRODUCTION

Open-channel junction flow is important in environmental and hydraulic engineering. It occurs in many hydraulic structures, such as irrigation systems, urban water supply and wastewater treatment facilities. The flow entering the lateral channel has complex specifications and leads to the creation of flow separation zones at the downstream corner of the junction. Different parameters effect in hydrodynamics of junction, flow that characterize the flow pattern. These include the shape, slope, angle between lateral and main channels and Froude numbers. In the past, study of junction flows has been performed using physical models, 1-D theoretical analysis, or 1-D numerical solutions. Taylor (1944) was probably the first one who applied an analytical model to open-channel junction flows. This model was able to predict the tributary channel depth upstream of the junction. Modi *et al.* (1981) calculated the size of the separation zone using a conformal mapping method under the assumption of in viscid and irrotational flow. A shape index of flow separation zone was obtained in the T-Junction with deviation different angles and discharge ratios by Best and Reid (1984). Chen and Lian (1992) simulated the geometry of T-junction using standard K-ε model with above Reynolds numbers. The results obtained for the ratio of small discharges had good agreement with experimental results, but in the higher discharges ratio, were significantly different from that of the measurements. Issa and Oliveira (1994) performed 3-D simulation of turbulent flow for T- shaped geometries. They solved Reynolds time-averaged Navier–Stokes equations (RANS) through K-ε-Standard model with wall functions. Ramamurthy *et al.* (2007) studied the transfer of lateral momentum from the branch channel to the main channel by measuring the pressure difference between the side banks of the branch channel. Biron *et al.* (1996) investigated the previously neglected effects of bed discordance on the channel junction flow. Hsu *et al.* (1998a) described a one-dimensional approach to predict the water depth upstream of the junction for a subcritical open channel and they were able to estimate the contraction coefficient at the maximum flow constriction. Their results correlated well with the available experimental data. Later, Hsu *et al.* (1998b) extended their previous model to investigate the flows in channels with different junction geometries, including of 30°, 40°, and 50° angles. Huang *et al.* (2002) numerically investigated water surface and flow velocity profiles at different sections of the main and lateral channel using k-ω turbulence model. Then, an empirical relation between the junction losses, the junction angle and discharge ratio were suggested. Ting *et al.* (2009) simulated the 90° equal-width open-channel junction flow using the 3-D k-ω model. Then applied to investigate the effect of the discharge ratio on the shape of separation zone cross-sectional mean flow angle and the contraction coefficient. The studies mentioned above provided useful information for understanding of the flow and engineering design of open-channel junctions. However, theoretical or numerical models aren't capable of taking some complex flow conditions into account such as effect of inflow Froude number on secondary flow and separation. In the present study, Froude number effects of the main and lateral channels entrance on flow separation zone are studied.

MATERIAL AND METHODS

For numerical simulation of the turbulent flow field, Fluent software with RSM turbulent model was used. Reynolds-averaged Navier–Stokes (RANS) equations are solved in addition to continuity equation. Quick and second Order Upwind schemes were used for solving momentums and turbulence equations, respectively. Moreover, standard method was used for discretization of pressure equation. Flow analysis occurring at persistent mode and PISO algorithm is used for velocity-pressure coupling. Method of discretization

of momentum equation, loss and turbulence kinetic energy and reynolds stress is done in second order upwind method. Also, standard method is used for discretization of pressure equation. The small values of the under-relaxation factors are required for the solution stability of the mentioned method, so the under-relaxation factors are chosen between 0.2 and 0.5. It should be noted that for calculating an unsteady free surface profile, a small initial time steps are required. Therefore, a time step between 0.01 and 0.1 are selected. Iterative convergences at every time step are checked and all residuals are dropped below three orders (1e-3). Solution procedure was continued until achieving 1e-4 for normalized residuals of each solved equation (Fluent Inc, 2006).

3-D continuity and momentum equations for turbulent flow are seen in the incompressible fluid, respectively (Fluent Inc, 2006).

$$\frac{\partial \overline{U_i}}{\partial x_i} = 0 \qquad (1)$$

$$\frac{\partial \overline{U_i}}{\partial t} + (\overline{U_j})\frac{\partial \overline{U_i}}{\partial x_j} = -\frac{1}{\rho}\frac{\partial \overline{p}}{\partial x_i} + g_{xi} + \frac{\partial}{\partial x_j}[(\nu + \nu_t)\frac{\partial \overline{U_i}}{\partial x_j}] \qquad (2)$$

where, 'U_i' and 'U_j' denote flow velocity in x and y directions, respectively, 't' is time, 'V and V_t' are molecular and turbulence viscosity, respectively, 'p' is pressure, 'k' is turbulence kinetic energy, 'ρ' is fluid density and 'g_{xi}' is gravity acceleration in the 'x_i' direction. Turbulent flows can be simulated using different turbulence models, including standard k-ε, RNG k-ε, Realizable k-ε, LES and the Reynolds-Stress Model (RSM), closure schemes. In the present study, Reynolds Stress Model (RSM) with standard wall function was selected for numerical simulations. The Volume Of Fluid (VOF) scheme is used for simulating free surface. In RSM turbulence model and tensor form of transport equation are as follows:

$$U_k \frac{\partial \overline{u_i' u_j'}}{\partial x_k} = P_{ij} + \Phi_{ij} + D_{ij} - \varepsilon_{ij} \qquad (3)$$

Where, $\overline{u_i' u_j'}$ is Reynolds stress, 'P_{ij}' is production tensor, 'ϕ_{ij}' is strain– pressure tensor, 'D_{ij}' is diffusion tensor and 'εij' is dissipation tensor (Fluent Inc, 2006).

In this study, the experimental data of Weber *et al.* (2001) were selected for validation of the numerical simulation. In experimental study of Weber *et al.*(2001), the main channel with the length of 21.95 m and the lateral channel with length of 3.66 m located at 90° have been investigated. The inlet velocities of lateral and main channels are equal to 0.5 m/s and 0.166 m/s, respectively. The outlet discharge of the main channel downstream is 0.17 m3/s, ratio of diverted discharge (q*) is 0.25, depth of downstream flow is 0.296 m Reynolds number (Re) is 186000 and width of both the channels (W) is 0.91 m. The simulation domain has been carefully chosen to represent the inflow and outflow boundaries. It is noted that the free-surface elevation is determined numerically and is not known before the computation. Therefore, the main channel length upstream of the branch channel is lengthened to 12W=10.92 m and the branch channel length is prolonged to 10W=9.10 m; so that, the fully developed flows are obtained near the downstream of the inlet boundaries. The length of main channel downstream of the branch channel is determined with 10W, where the flow depth is nearly constant (Weber, 2001).

In 3-D simulations performed in the present study, the boundaries depending on the nature of the flow were solid walls, inlet, outlet and free-surface. Two separate inlets were specified for air and water that at each inlet, uniform distributions were given for all of dependent variables. The water velocity was defined at the inlet section with a known water depth entering the flow domain and inlet discharge and the applied air velocity at the flow inlet was equal to 1e-5 m/s. The

turbulence kinetic energy (k_0) and dissipation rate (ε_0) at the inlet boundary were estimated by the following equations (Fluent Inc, 2006):

$$k_0 = \frac{3}{2}(T_u U_0)^2 \quad (4)$$

$$\varepsilon_0 = C_\mu^{3/4} \frac{k^{3/2}}{l} \quad (5)$$

Here, 'U_O' refers the average inlet velocity, 'T_u' denotes the turbulence intensity which is typically between 1% and 5% and it depends on the upstream flow. '$C\mu$' represents constant and it is equal to 0.09 and ldenotes0.07D_h in which D_h is the hydraulic diameter. At the air surface, symmetry conditions were applied which enforce a zero normal velocity and a zero shear stress there. To estimate the wall effects on the flow, empirical wall functions known as standard wall functions were used. The RSM model utilized the wall functions approach for linking the gaps between the logarithmic layer and the near-wall viscous sub layer.

Appropriate meshing of regional flow exists is also one of the important parameters in the run time model. Figure 1 shows the three-dimensional plan and view of computational domain meshing in the 90^0junction.Thedimension of cells number of computational domain meshing in the x, y and z directions in zones 1, 2, 3 and 4 are 47×40×22, 40×40×22, 47×40×22 and 40×48×22, respectively. A finer mesh used did not show an appreciable difference in the results.

RESULTS

Evaluation of water surface profiles

In this section, water surface profiles in different cross-sections of the main channel are investigated for constant discharge ratio of 0.25. In Figure 2, the dimensionless water surface profiles (Z*), for different cross-sections of the main channel for discharge ratio of 0.25areillustrated. X^*,$Y^{**}$and Z* are distances at x, y and z axes, respectively which have become dimensionless by the width of lateral and main channels.

According to Figure 2, water surface profiles at different sections of the main channel are compared with the experimental results and a good agreement is found between them. It is seen that similar results of Ting *et al.* (2009), the surface elevation nearer to the branch channel (with less Y*) has more smart depression. Table 1 presents the mean error percentage obtained from the

Table 1. The mean error percentage obtained from the comparison of the numerical values with experimental

Section	Y*=0.167	Y*=0.333	Y*=0.500	Y*=0.667	Y*=0.883
Present Study	0.72	1.25	1.36	0.52	0.63
Ting *et al.* (2009)	2.01	3.08	3.68	1.61	0.55

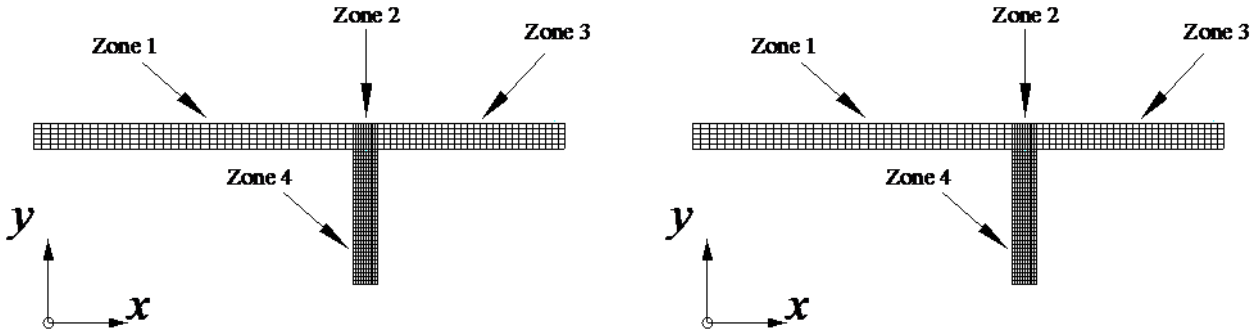

(a) (b)

Figure 1. **Computational geometry and grid, a) plan and b) three-dimensional view**

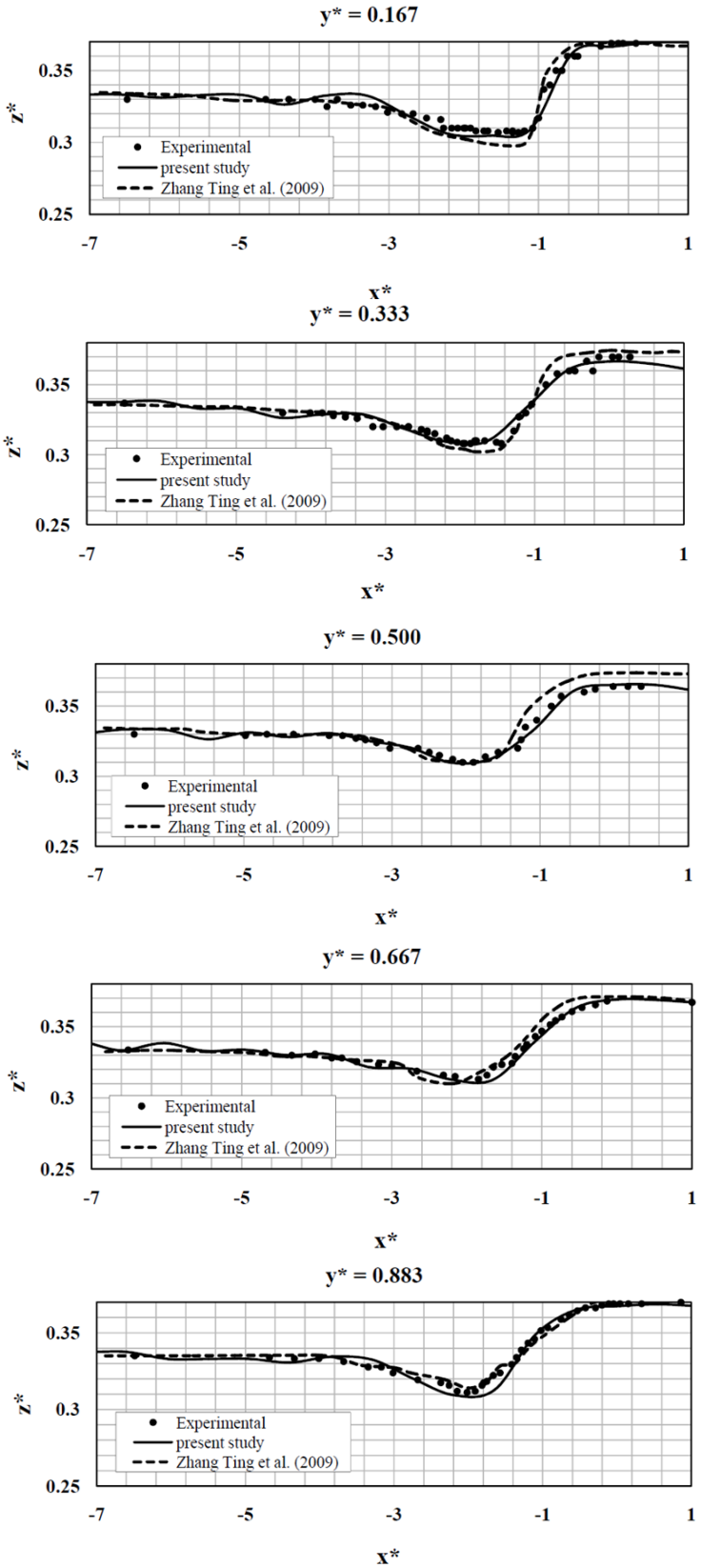

Figure 2. Comparison of water surface elevation profiles

comparison of the numerical values resulted from the present study and Ting *et al.*(2009) study with experimental values at different sections of the main channel. For error percentage calculation, Root Mean

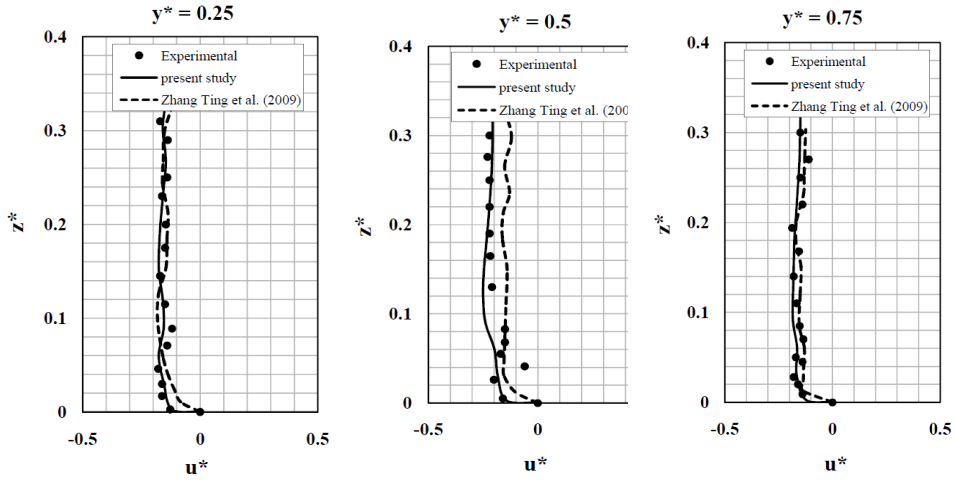

Figure 3. Comparison of computational velocity profiles at X*=1 in main channel

Square Error method (RMSE) is used. The RMSE of a model prediction with respect to the estimated variable X_{model} is defined as the square root of the mean squared error:

$$RMSE = \sqrt{\frac{\sum_{i=1}^{n}(X_{obs,i} - X_{model,i})^2}{n}} \qquad (5)$$

Where 'X_{obs}' is observed values and 'X_{model}' is modeled values at time/place 'I'.

According to Table 1, in all sections except section Y*=0.883, present study results have better agreement with the experimental results than Ting *et al.* (2009) results. It indicates the high ability of this numerical model in predicting distribution of water surface elevation profiles.

In continue, flow velocity profiles in different cross-sections of the junction are investigated for constant discharge ratio 0.25. In Figures 3 to 6, the dimensionless velocity profiles (U_x/U_0) near the water

Table 2. The mean error percentage obtained from the comparison of the numerical values with experimental

Section	x*=1			x*=-1			x*=-6		y*=-1			
	y*=0.25	y*=0.5	Y*=0.75	y*=0.25	y*=0.5	y*=0.75	y*=0.25	y*=0.5	y*=0.75	x*=-0.25	x*=-0.5	x*=-0.75
Present Study	1.54	1.89	1.58	0.78	1.75	1.90	1.01	2.43	2.55	2.86	3.07	2.52
Ting *et al.* (2009)	2.01	6.64	1.85	3.92	9.11	6.80	4.05	12.12	5.10	7.00	6.93	6.02

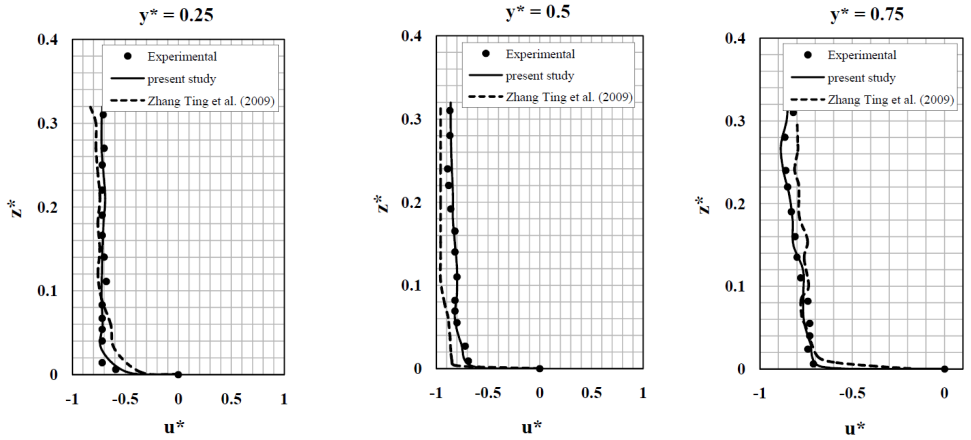

Figure 4.Comparison of computational velocity profiles at X*= -1 in main channel

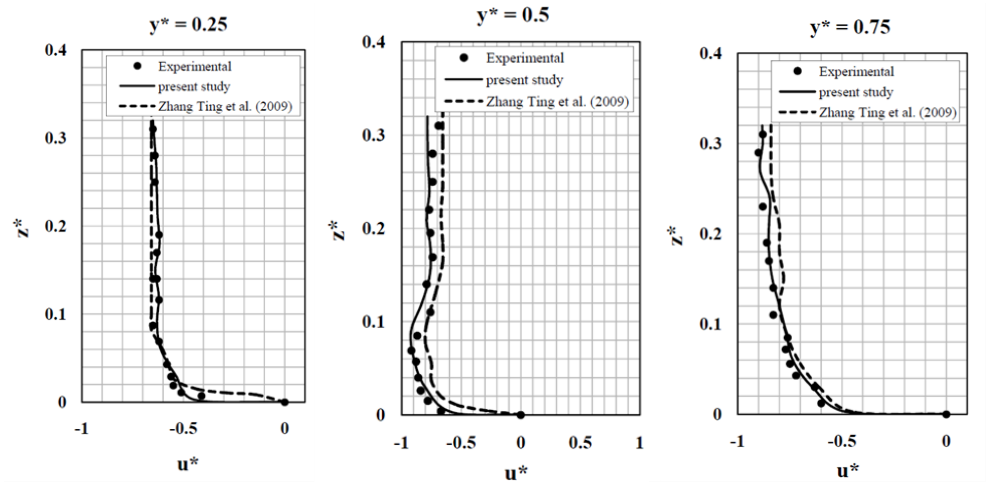

Figure 5. Comparison of computational velocity profiles at X*= -6 in main channel

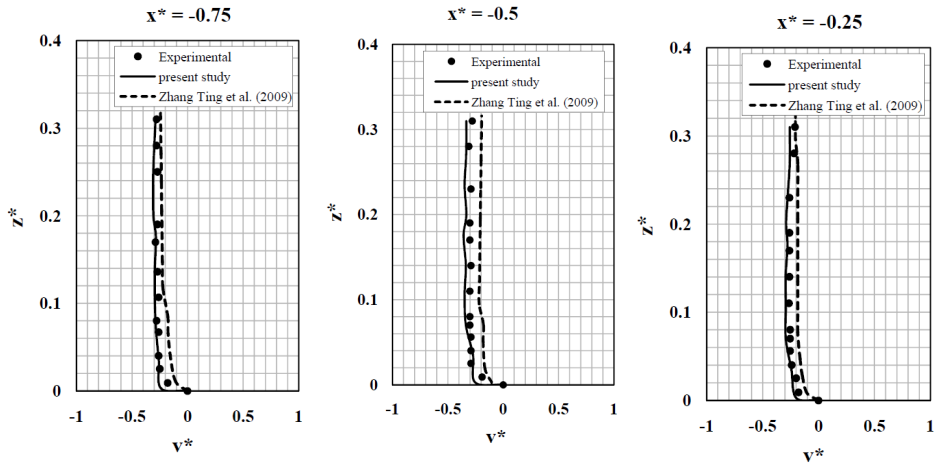

Figure 6. Comparison of computational velocity profiles atY*= -1 in main channel

level, for different cross-sections of the lateral and main channels are shown. 'U_0' is the maximum velocity at the cross-section X*=4.65 whose value is equal to 0.28 m/s.

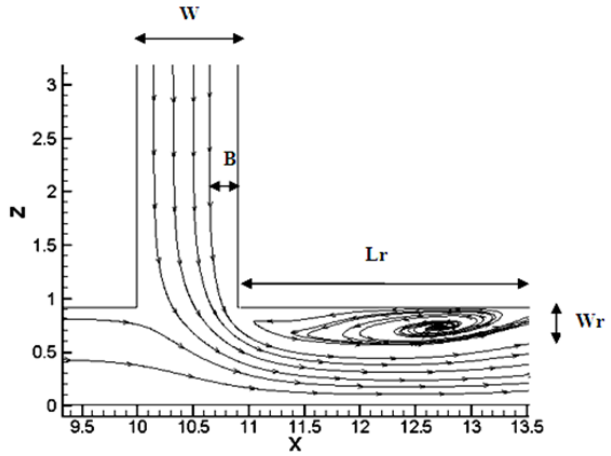

Figure 7. Circulation zone in main channel and parameters definition

Figure 3 shows the upstream regions of main channel (at X*=1) here, the velocity is evenly distributed across the section. Due to the momentum inflow of lateral channel and the influence of separation zone, the flow in the junction region shifts to the wall opposite to the junction and the flow distribution is quite non-uniform (Figure 6). At the location of Y*=0.25, it is apparent that higher velocities occur near the bed. Similar results of Ting *et al.* (2009) downstream of the separation zone (X*=-6), flow begins to recover from the effect of separation and to distribute more evenly. For completeness of the comparison, the transverse velocity in the lateral channel is also compared in Figure8. The results indicated that transverse velocity is very small in

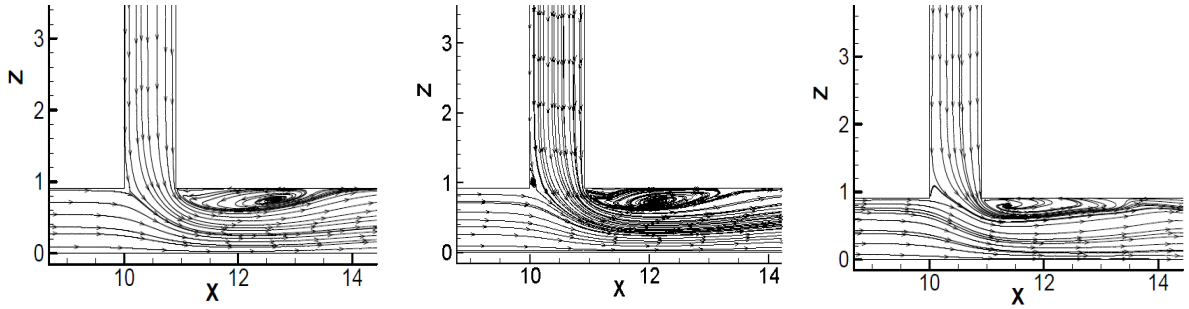

Figure 8. Streamlines in different depths for constant Froude number of main channel entrance 0.37

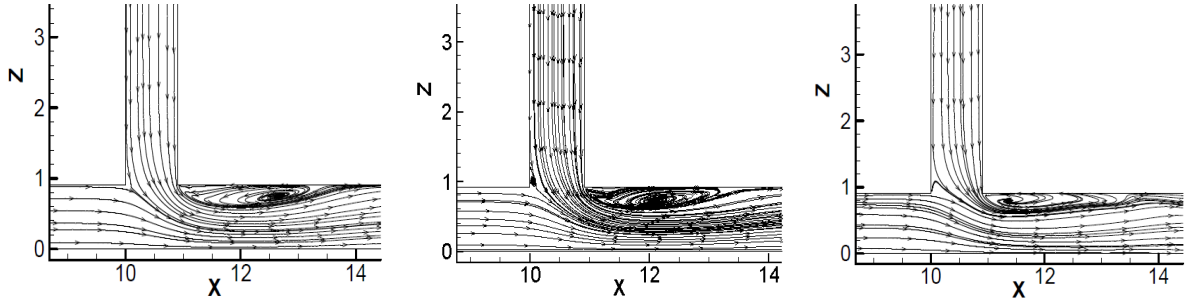

Figure 9. Streamlines in different depths for constant Froude number of lateral channel entrance 0.37

the upstream of the branch channel (Y*=-1), indicating that the secondary flow is negligible at these cross sections. However, transverse velocity close to the junction starts to increase, indicating that the secondary flow is quite strong (Issa and Oliveira, 1994).

Table 2 shows the mean error percentage obtained from the comparison of the numerical values resulted from the present study with experimental values at different sections of the lateral and main channels. According to Table 2, in all sections, present study results have better agreement with the experimental results than Ting *et al.* (2009) results. Average RMSE obtained of the Ting *et al.* (2009) was 5.94% while in present study this amount was 1.97%.

DISCUSSION

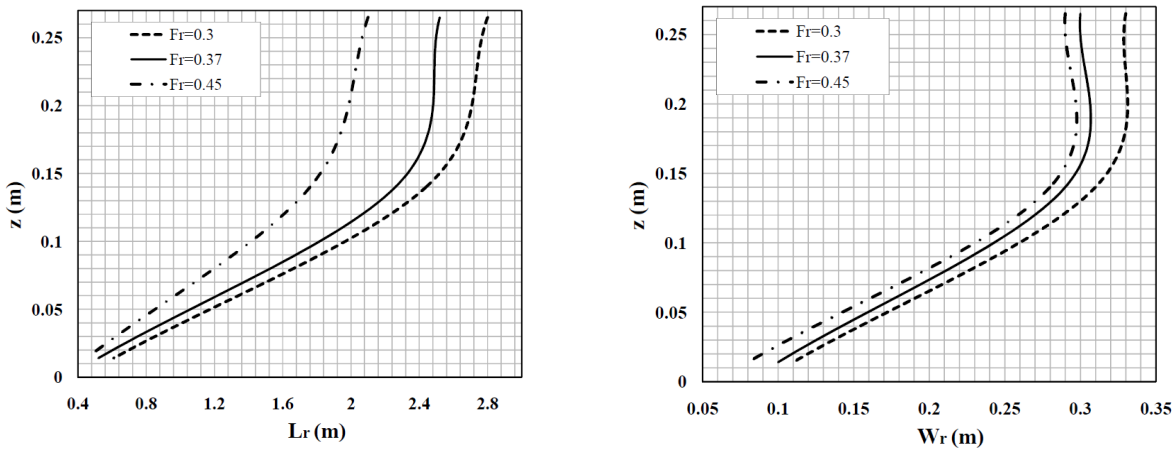

Figure 10. Changes of the flow separation zone dimensions in different depths for different Froude numbers of main channel entrance

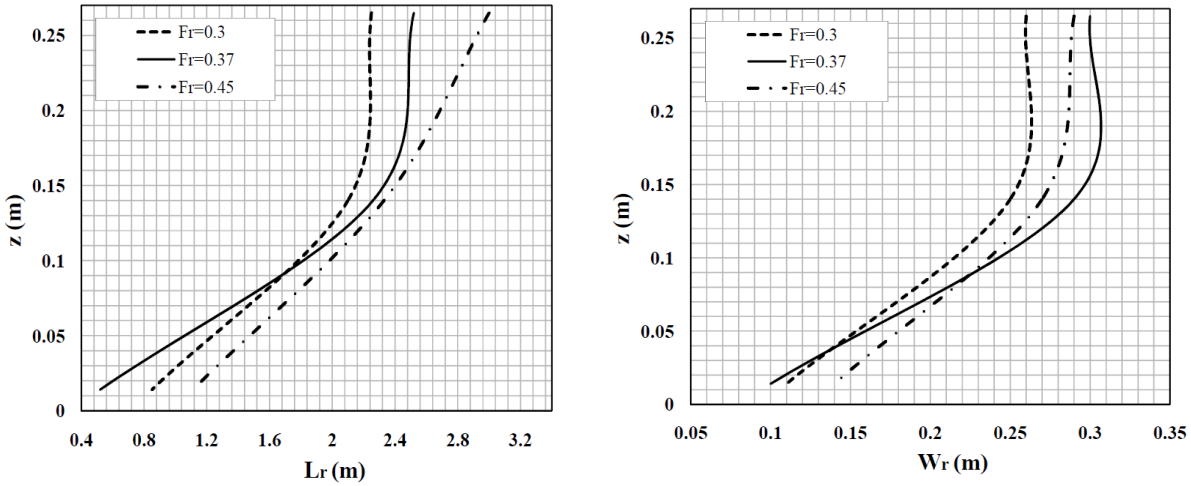

Figure 11. Changes of the flow separation zone dimensions in different depths for different Froude numbers of lateral channel entrance

Figure 7 shows circulation zone in main channel and different parameters. In this Figure, 'L_r, W_r and B' are length and width of circulation zone and stream tube width, respectively.

Figures 8 and 9 show streamlines near the water surface, middle depth and near the bed for constant Froude number of main and lateral channels entrance (Fr).

According to the Figures 8 and 9, Figures 10 and 11 show changes of the flow separation zone dimensions in different depths for different Froude numbers of main and lateral channels entrance, respectively.

According to the Figures 10 and 11, Froude numbers of main and lateral channels entrance are important parameters on length and width of circulation zone in different depths and their increasing leads to the increase of length and width of circulation zone. For a ratio of constant discharge, with approaching to channel bed, length of circulation zone decreases. Also, width of circulation zone at near the water surface is larger than near the bed.

CONCLUSION

At this study, the numerical simulation flow was performed in a 90^0 junction and Navier-Stokes equations were solved by Finite-Volume Method. Water surface profiles at different sections of the main channel were compared with the experimental and numerical results of other researchers; and a good agreement was found between them. In the upstream regions of main channel, the velocity is evenly distributed across the section. Downstream of the separation zone (X*=-6), flow begins to recover from the effect of separation and to distribute more evenly.

For the ratio of constant discharge with respect to channel bed, length of circulation zone decreases. Also, width of circulation zone nearer to the water surface is larger than the bed. With increasing Froude number of the main and lateral channels entrance, stream tube dimensionless width in water surface and bed increases and decreases, respectively.

REFERENCES

Best JL and Reid I. (1984). Separation zone at open-channel junctions. *Journal of Hydrologic Engineering,* ASCE, 110(11):1588-1594.

Biron P, Best JL and Roy AG. (1996). Effects of Bed Discordance on flow dynamics at open channel confluences. *Journal of Hydraulic Engineering*, 122 (12):676–682.

Chen HB and Lian GS. (1992). The numerical

computation of turbulent flow in T-junction. *Journal of Hydrodynamics,* 3:50-58.

Fluent Inc. (2006). Fluent 6.3.26 User Manual. Lebanon: Fluent Inc.

Hsu CC, Wu FS and Lee WJ. (1998). Flow at 90° equal-width open-channel junction. *Journal of Hydraulic Engineering*, 124(2), 186.

Huang J, Weber LJ and Lai YG. (2002). Three-dimensional numerical study of flows in open-channel junctions. *Journal of Hydrologic Engineering,* ASCE, 128(3):268-280.

Issa RI and Oliveira PJ. (1994). Numerical prediction of phase separation in two-phase flow through T-junctions. *Computers and Fluids,* 23(2):347-372.

Modi RN, Dandekar MM and Ariel RD. (1981). Conformal mapping for channel junction flow. *Journal of Hydraulic Engineering*, 107(12):1713–1733.

Ramamurthy AS, Junying Qu and Diep Vo. (2007). Numerical and experimental study of dividing open-channels Flows. *Journal of Hydraulic Engineering,* 133 (10):1135-1144.

Taylor EH. (1944). Flow characteristics at rectangular open-channel junctions. *Transactions of the American Society of Civil Engineers*, 109(1): 893–902.

Weber LJ, Schumate ED and Mawer N. (2001). Experiments on flow at a 90^{o} open-channel junction [J]. *Journal of Hydraulic Engineering,* ASCE, 127(5): 340-350.

Zhang Ting, Wei-Lin Xu and Chao Wu. (2009). Effect of discharge ratio on flow characteristics in 90^{0} equal-width open-channel junction. *Journal of Hydrodynamics,* Science Direct, 21(4):541-549.